·X-Ray Crystallographic Analysis

X-ray electron density distribution analysis of [1·C_6H_6]:

Crystal data: $C_{52}H_{102}Si_{10}·C_6H_6$, FW = 1086.34, orthorhombic *Pnna*, a = 18.1857(3), b = 30.4174(5), c = 12.6976(2) Å, V = 7023.8(2) Å^3; D_X = 1.027 g cm^{-3}; Z = 4; μ(0.30241 Å) = 0.035 mm^{-1}, T = 90 K.

A yellow block-shaped single crystal of [**1**·C_6H_6] (size: 0.40 × 0.35 × 0.20 mm^3) was selected for the measurements. The diffraction data were collected with a large cylindrical imaging plate camera installed at the BL02B1 beamline of SPring-8 by an oscillation method about the ω-axis at 90 K using Si(111) monochromated X-rays (λ = 0.30241(12) Å). Bragg spots were integrated, scaled, and averaged up to $\sin\theta / \lambda$ = 1.25 Å^{-1} using the program PROCESS-AUTO.[S1] Lorentz, polarization, and empirical absorption corrections were applied. The number of measured and independent reflections, completeness, and R_{int} were 305534, 57329, 0.997, and 0.0383, respectively.

The initial structure of [**1**·C_6H_6] was solved by a direct method using the program SIR2004[S2] and refined by a full-matrix least-squares method using the program SHELXL-2018/3.[S3] Positions of H atoms were located on difference Fourier maps, except those in the disordered substituents, which were generated with geometrical calculations and refined by applying riding models.

High-order refinements were carried out using 50966 independent reflections with $\sin\theta / \lambda \geq 0.60$ Å^{-1}. The C–H distance was constrained at 1.059, 1.099, and 1.083 Å for methyl, methine, and aromatic moieties, respectively, on the refinements.

The multipole refinements using the Hansen-Coppens multipole formalism[S4] and topological analysis based on the resulting parameters were performed with the XD2016 package.[S5] The refinements were carried out against 23210 independent reflections with $I > 3\sigma(I)$ at $\sin\theta / \lambda \leq 1.00$ Å^{-1} (R_{int} = 0.0298 for 29319 independent reflections) based on F^2. At the first stage of the refinements, the atomic coordinates and temperature factors of the atoms were fixed to those from high-order refinement. The population parameters, P_v, $P_{lm\pm}$ of the non-hydrogen atoms, and scale were refined. The multipole level of population parameters was raised up to hexadecapole for the Si atoms, octupole for the C atoms, and dipole along with the C−H bonds for the H atoms. Chemical equivalent constraints were imposed for multipole parameters of all atoms. The radial screening parameters (κ and κ' for the Si and the H atoms) were fixed at 1.0 and 1.1, respectively, and those of the C atoms were refined after refinements of multipole parameters at the highest level of each atom. The refinement cycles were repeated until parameters converged. During the second stage, the temperature factors were refined by applying the Gram-Charlier 4th order anharmonic models for the Si atoms in the Tbb ligands except those in the minor part of the disordered Tbb, which were fixed at the result of the high-order refinements, harmonic anisotropic models for the other non-H atoms, and isotropic models for the H atoms, following the refinements of the radial screening parameters, κ and κ'. The chemical equivalent constraints on the multipole parameters for the non-H atoms were released. The stage was repeated until the shifts of the parameters converged. During the final stage, the coordinates, harmonic temperature factors, and multipoles were refined. The C−H distances were fixed at 1.059, 1.099, and 1.083 Å for methyl, methine, and aromatic moieties, respectively. The number of parameters in the final cycle of the refinements was 996. The total molecular charges of **1** and the solvated benzene were constrained to be each neutral. The final R factors were 0.0276 and 0.0497 for $R(F)$ and $wR(F^2)$, respectively (23210 reflections with $I > 3\sigma(I)$). The lowest and highest residual densities were −0.32 and 0.64 e·Å^{-3},

respectively. Supplementary crystallographic data were deposited at the Cambridge Crystallographic Data Centre (CCDC) under reference number CCDC 2170207 and can be obtained free of charge *via* https://www.ccdc.cam.ac.uk/structures.

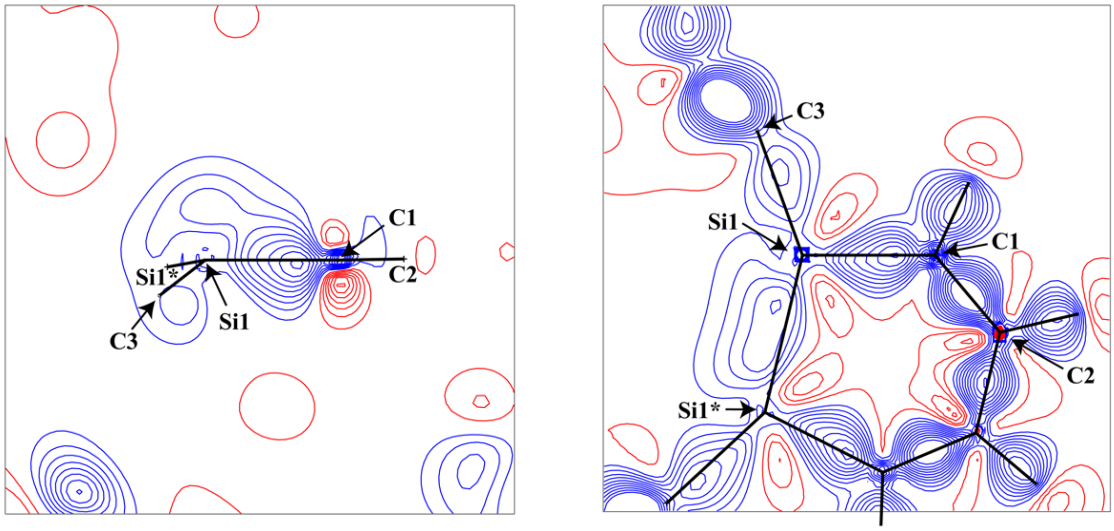

(a) Si1-C1 π-plane **(b) Perpendicular to Si1-C1 π-plane**

Fig. S1. Static model maps of 1,2-disilabenzene **1** from (a) the side-view of Si1–C1 π-plane and (b) the top-view perpendicular to Si1–C1 π-plane. Blue and red contours denote positive and negative electron density, respectively, drawn at 0.05 e Å^{-3} intervals.

X-ray electron density distribution analysis of [2·C$_6$H$_6$]:

Crystal data: $C_{52}H_{102}Ge_2Si_8 \cdot C_6H_6$, *FW* = 1175.34, orthorhombic *Pnna*, *a* = 18.2272(10), *b* = 30.5096(16), *c* = 12.6275(7) Å, *V* = 7022.2(7) Å^3; D_X = 1.112 g cm^{-3}; *Z* = 4; μ(0.31979 Å) = 0.127 mm^{-1}, *T* = 90 K.

A yellow block-shaped single crystal of [**2·C$_6$H$_6$**] (size: 0.20 × 0.18 × 0.15 mm^3) was selected for the measurements. The diffraction data were collected with a large cylindrical imaging plate camera installed at the BL02B1 beamline of SPring-8 by an oscillation method about the ω-axis at 90 K using Si(111) monochromated X-rays (λ = 0.319789(12) Å). Bragg spots were integrated, scaled, and averaged up to $\sin\theta / \lambda$ = 1.25 Å^{-1} using the program PROCESS-AUTO.[S1] Lorentz, polarization, and empirical absorption corrections were applied. The number of measured and independent reflections, completeness, and R_{int} were 305534, 57329, 0.997, and 0.0383, respectively.

The initial structure of [**2·C$_6$H$_6$**] was solved by a direct method using the program SIR2004[S2] and refined by a full-matrix least-squares method using the program SHELXL-2018/3.[S3] Positions of H atoms were located on difference Fourier maps, except those in the disordered substituents, which were generated with geometrical calculations and refined by applying riding models.

High-order refinements were carried out using 50966 independent reflections with $\sin\theta / \lambda \geq 0.60$ Å^{-1}. The C–H distance was constrained to 1.059, 1.099, and 1.083 Å for methyl, methine, and aromatic moieties, respectively, on the refinements.

The multipole refinements using the Hansen-Coppens multipole formalism[S4] and topological analysis based on

the resulted parameters were performed with the XD2016 package.[S5] The refinements were carried out against 23210 independent reflections with $I > 3\sigma(I)$ at $\sin\theta / \lambda \leq 1.00$ Å^{-1} ($R_{int} = 0.0409$ for 29407 all independent reflections) based on F^2. During the first stage of the refinements, the atomic coordinates and temperature factors of the atoms were fixed on those from high-order refinement. The population parameters, P_v, $P_{lm\pm}$ of the non-hydrogen atoms, and scale were refined. The multipole level of population parameters was raised up to hexadecapole for the Ge and the Si atoms, octupole for the C atoms, and dipole along with the C−H bonds for the H atoms. Chemical equivalent constraints were imposed for multipole parameters of all atoms. The radial screening parameters (κ and κ' for the Si and the H atoms) were fixed at 1.0 and 1.1, respectively, and those of the C atoms were refined after refinements of multipole parameters at the highest level of each atom. The refinement cycles were repeated until parameters converged. During the second stage, the temperature factors were refined by applying the Gram-Charlier 4th order anharmonic models for the Ge and the Si atoms, except those in the minor part of the disordered Tbb, which were fixed at the result of the high-order refinements, harmonic anisotropic models for the other non-H atoms, and isotropic models for the H atoms, following the refinements of the radial screening parameters (κ and κ'). The chemical equivalent constraints on the multipole parameters for the non-H atoms were released. This stage was repeated until the shifts of the parameters converged. During the final stage, the coordinates, temperature factors, and multipoles were refined. The C−H distances were fixed at 1.059, 1.099, and 1.083 Å for methyl, methine, and aromatic moieties, respectively. The number of parameters in the final cycle of the refinements was 1151. Total molecular charges of **2** and the solvated benzene were constrained to be each neutral. The final R factors were 0.0162 and 0.0345 for $R(F)$ and $wR(F^2)$, respectively, for 24835 reflections with $I > 3\sigma(I)$. The lowest and highest residual densities were −0.24 and 0.51 e·Å^{-3}, respectively. Supplementary crystallographic data were deposited at the Cambridge Crystallographic Data Centre (CCDC) under reference number CCDC 2170208 and can be obtained free of charge *via* https://www.ccdc.cam.ac.uk/structures.

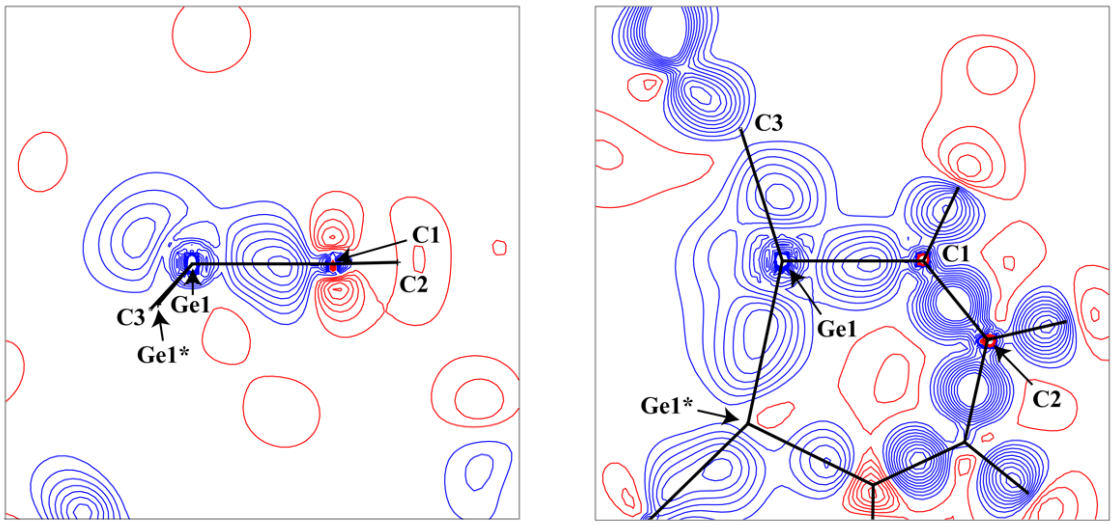

(a) Ge1-C1 pi-plane **(b) Perpendicular to Ge1-C1 pi-plane**

Fig. S2. Static model maps of 1,2-digermabenzene **2** from (a) the side-view of Ge1–C1 π-plane and (b) the top-view perpendicular to Ge1–C1 π-plane. Blue and red contours denote positive and negative electron density, respectively, drawn at 0.05 e Å^{-3} intervals.

· Bader AIM analysis including *H* (total electron energy density), *G* (kinetic energy density), and *V* (potential energy density).

Table S1. Bader AIM analysis

[**1**·C_6H_6]	ρ_{BCP} / e Å^{-3}	$\nabla^2\rho$ / e Å^{-5}	H/ Hartree Å^{-3}	G/ Hartree Å^{-3}	V/ Hartree Å^{-3}	ε
Si1–Si1*	0.667(17)	-3.08(2)	-0.48	0.27	-0.75	0.09
Si1–C1	0.96(2)	-0.74(7)	-0.77	0.72	-1.49	0.65
C1–C2	2.17(2)	-20.02(5)	-3.39	1.99	-5.38	0.32
C2–C2*	1.95(2)	-17.46(4)	-2.85	1.62	-4.47	0.33
C31–C32	2.36(5)	-24.1(1)	-3.92	2.24	-6.16	0.31
C32–C33	2.16(6)	-24.4(3)	-3.47	1.76	-5.24	0.10
C33–C34	2.24(4)	-21.89(8)	-3.59	2.05	-5.64	0.41
[**2**·C_6H_6]	ρ_{BCP} / e Å^{-3}	$\nabla^2\rho$ / e Å^{-5}	H/ Hartree Å^{-3}	G/ Hartree Å^{-3}	V/ Hartree Å^{-3}	ε
Ge1–Ge1*	0.814(17)	-1.88(3)	-0.61	0.48	-1.10	0.34
Ge1–C1	1.036(19)	0.20(4)	-0.85	0.86	-1.71	0.12
C1–C2	2.241(12)	-23.55(3)	-3.63	1.99	-5.62	0.18
C2–C2*	2.089(14)	-20.41(2)	-3.22	1.79	-5.01	0.16
C31–C32	2.13(2)	-20.10(5)	-3.31	1.90	-5.21	0.14
C32–C33	2.02(2)	-19.62(6)	-3.04	1.67	-4.71	0.17
C33–C34	2.228(18)	-23.39(3)	-3.60	1.97	-5.57	0.22

The positive Laplacian ($\nabla^2\rho$) value at the bond critical point (BCP) of the Ge1-C1 bond in **2** results from the different number of electrons in Ge and C atoms. The Laplacian value at a BCP is defined as the sum of three curvatures in orthogonal direction relative to each other, where one (λ_3) coincides with the bond direction, while the others (λ_1 and λ_2) are aligned perpendicular to the bond and to each other. While λ_3 is positive, the λ_1 and λ_2 are negative at the BCP. In the case of the covalent bonds between the heavier and the second raw elements, owing to the large difference in the number of electrons between the atoms and less concentrated bonding electron density than those in the case between the second raw elements, the λ_3 becomes a large positive value and the λ_1 and λ_2 become small negative values. The Laplacian value as the sum of these curvatures is calculated as small negative or small positive, the former case is for **1** and the latter case is for **2**.

In addition to the Laplacian value at the BCP to characterize the bonding nature, total energy density (H) is widely used.[S6] The H value is derived as the sum of kinetic energy density (G) and potential energy density (V). According to Bader, if the Laplacian is positive and H is negative, the bond can be characterized as closed-shell interaction with covalency, which shows clear contrast with the characterization with only the Laplacian value.

·Computational calculations.

NICS calculations were carried out using the *Gaussian 16* (Revision C.01) program package.[S7] The geometries of **1** and **2** obtained from the single-crystal XRD analyses were used. The theoretical levels are indicated in the main text. The calculated HOMOs and LUMOs of **1** and **2** are shown in Fig S3.

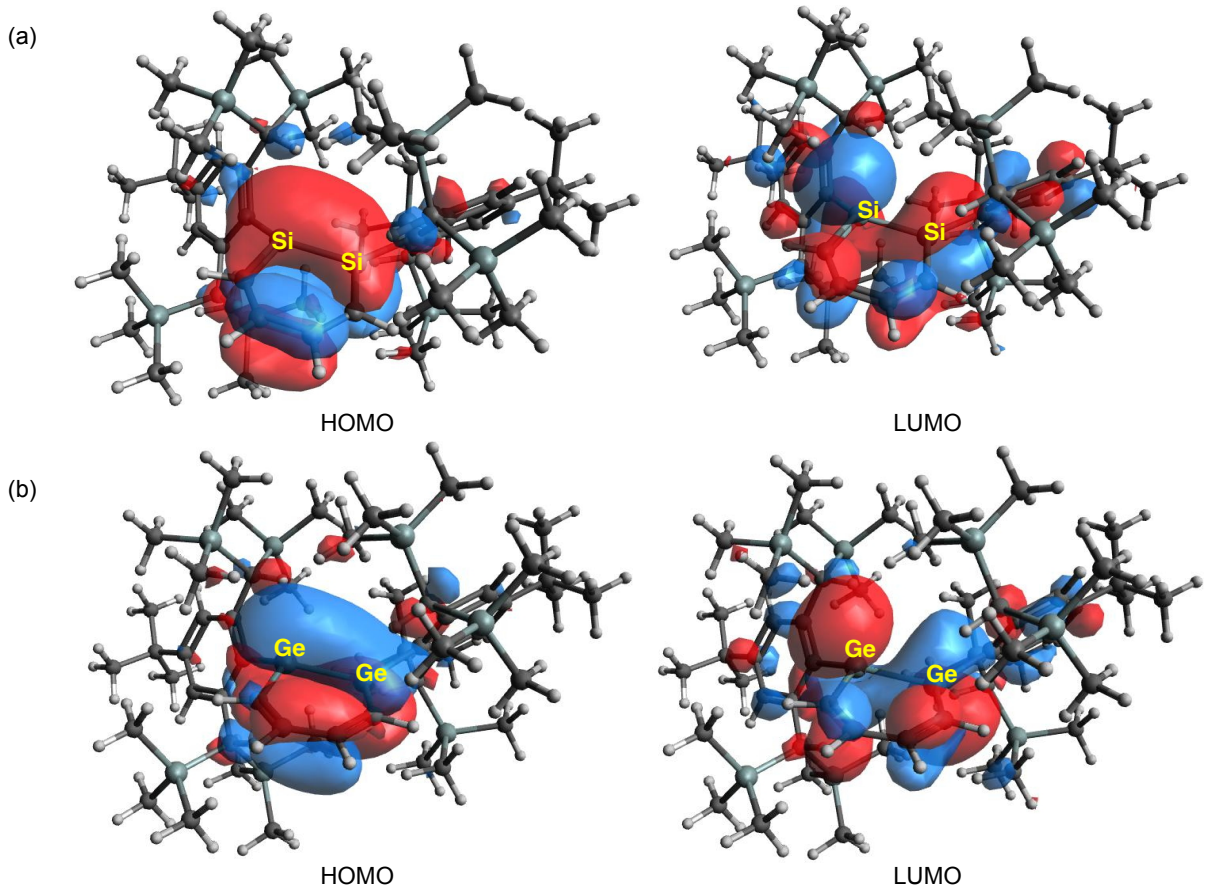

Fig. S3. Frontier orbitals of (a) 1,2-disilabenzene **1** and (2) 1,2-digermabenzene **2** calculated at the B3PW91-D3(BJ)/6-311G(3df,p) level of approximation.

Geometries of 1,2-disilabenzene and 1,2-digermabenzene derivatives were taken from their single-crystal X-ray crystallographic data. Aryl substituents involving bulky groups were replaced by Ph groups, and then only the positions of those hydrogen atoms that replace the bulky groups were replaced were optimized at the RB3LYP/cc-pVDZ level of approximation. We then evaluated the nucleus-independent chemical shift (NICS) values as well as the aromaticity of the induced-current density (ACID) plot as metrics of the aromatic character at the GIAO-/CSGT-LC-RBLYP(μ = 0.33 bohr^{-1})/cc-pVTZ level of approximation. It should be noted here that LC-UBLYP solutions of these systems are found to reduce the LC-RBLYP solutions. Molecular coordinates and the direction of the magnetic field during the ACID calculations were set as shown in Fig. S4. We also analyzed the delocalization effects from the critical isosurface values (CIVs)[S8,S9] between the E-E bonds (Fig. S4). Higher CIVs correspond to stronger conjugation between the atoms. The CIV of benzene is calculated to be 0.089 at the present level of approximation (LC-RBLYP(μ = 0.33 bohr^{-1})/cc-pVTZ) and is in good agreement with a previously reported value (0.0898 at the M06-2X/6-31G(d) level[S10]). The obtained results of CIVs indicate that the degrees of electron delocalization between the E-E bonds are lower in 1,2-disilabenzene (Si-Si, 0.037) and 1,2-digermabenzene (Ge-Ge, 0.036) than that in benzene (C-C, 0.089), whereby the CIV of the 1,2-digermabenzene is slightly smaller than that of the 1,2-disilabenzene.

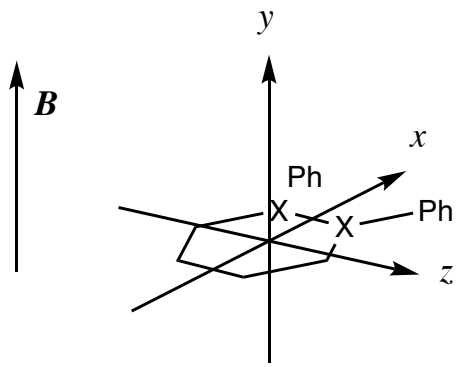

Fig. S4. Molecular coordinates and the direction of magnetic field for the ACID calculation.

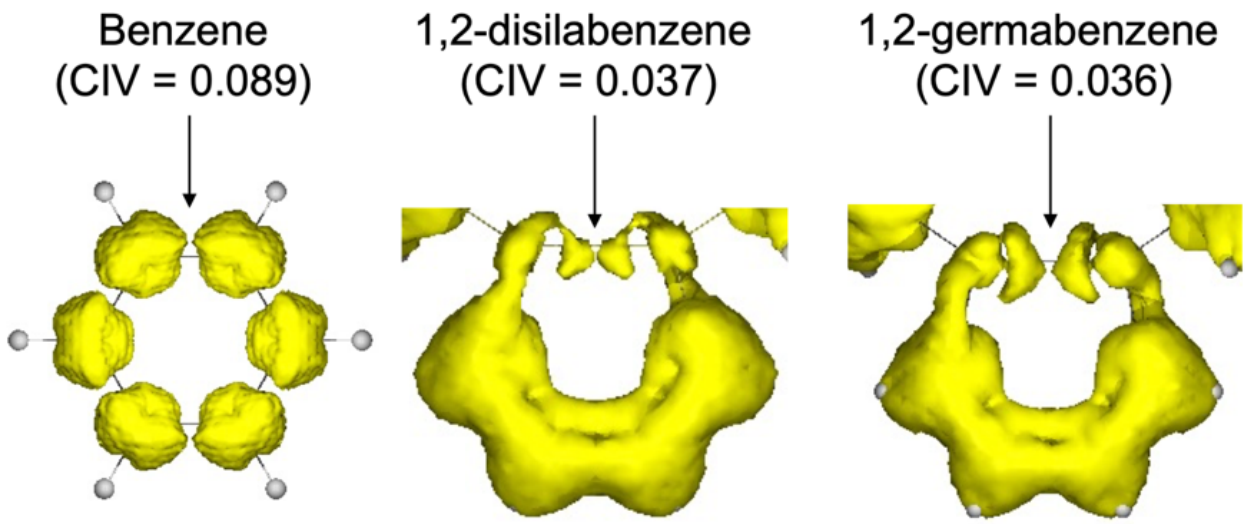

Fig. S5. Critical isosurface values (CIVs) for the ACID scalar field.

References

(S1) PROCESS-AUTO (1998). Automatic Data Acquisition and Processing Package for 2D image data. Rigaku Corporation, Tokyo, Japan.

(S2) M. C. Burla, R. Caliandro, M. Camalli, B. Carrozzini, L. Cascarano, L. De Caro, C. Giacovazzo, G. Polidori, R. Spagna, *J. Appl. Cryst.* 2005, **38**, 381-388.

(S3) G. M. Sheldrick, *Acta Cryst.*, 2015, **C71**, 3-5.

(S4) N. K. Hansen, Coppens, P., *Acta Cryst.*, 1978, **A34**, 909-921.

(S5) XD2016 – A Computer Program Package for Multipole Refinement, Topological Analysis of Charge Densities and Evaluation of Intermolecular Energies from Experimental and Theoretical Structure Factors, A. Volkov, P. Macchi, L. J. Farrugia, C. Gatti, P. Mallinson, T. Richter, T. Koritsanszky (2016).

(S6) R. F. W. Bader, *Atoms in Molecules – A Quantum Theory*, Oxford University Press, New York, 1990.

(S7) M. J. Frisch, G. W. Trucks, H. B. Schlegel, G. E. Scuseria, M. A. Robb, J. R. Cheeseman, G. Scalmani, V. Barone, G. A. Petersson, H. Nakatsuji, X. Li, M. Caricato, A. V. Marenich, J. Bloino, B. G. Janesko, R. Gomperts, B. Mennucci, H. P. Hratchian, J. V. Ortiz, A. F. Izmaylov, J. L. Sonnenberg, D. Williams-Young, F. Ding, F. Lipparini, F. Egidi, J. Goings, B. Peng, A. Petrone, T. Henderson, D. Ranasinghe, V. G. Zakrzewski, J. Gao, N. Rega, G. Zheng, W. Liang, M. Hada, M. Ehara, K. Toyota, R. Fukuda, J. Hasegawa, M. Ishida, T. Nakajima, Y. Honda, O. Kitao, H. Nakai, T. Vreven, K. Throssell, J. A. Montgomery, Jr., J. E. Peralta, F. Ogliaro, M. J. Bearpark, J. J. Heyd, E. N. Brothers, K. N. Kudin, V. N. Staroverov, T. A. Keith, R. Kobayashi, J. Normand, K. Raghavachari, A. P. Rendell, J. C. Burant, S. S. Iyengar, J. Tomasi, M. Cossi, J. M. Millam, M. Klene, C. Adamo, R. Cammi, J. W. Ochterski, R. L. Martin, K. Morokuma, O. Farkas, J. B. Foresman and D. J. Fox, *Gaussian 16, Revision C.01,* , 2016, Gaussian, Inc., Wallingford CT, 2016.

(S8) D. Geuenich, K. Hess, F. Kohler, R. Herges, *Chem. Rev.*, 2005, **105**, 3758-3772.

(S9) R. Herges, D. Geuenich, *J. Phys. Chem. A* 2001, **105**, 3214-3220.

(S10) R. A. Matute, P. Pérez, E. Chamorro, N. Villegas-Escobar, D. Cortés-Arriagada, B. Herrera, S. Gutiérrez-Oliva, and A. Toro-Labbé, *J. Org. Chem.* 2018, **83**, 5969-5974.